Proceedings of the 9th World Congress on Momentum, Heat and Mass Transfer (MHMT 2024)
London, United Kingdom – April 11 – 13, 2024
Paper No. ICMFHT 122
DOI: 10.11159/icmfht24.122

Physics Informed Neural Network in Turbulent Porous Flow: Pore-scale Flow Reconstruction

Seohee Jang[1], Mohammad Jadidi[2], Yasser Mahmoudi[3]
[1]seohee.jang@postgrad.manchester.ac.uk; [2]mohammad.jadidi@manchester.ac.uk; [3]yasser.mahmoudi@manchester.ac.uk
Department of Fluids & Environment, University of Manchester, M13 9PL, United Kingdom

Abstract **-** Turbulence modelling in porous media presents challenges in Computational Fluid Dynamics (CFD). While various modelling approaches have been employed to analyze turbulent flow properties, achieving both precision and cost-effectiveness remains a significant hurdle. In recent years, Deep Learning (DL), with its capacity for solving nonlinear model, has emerged as a promising solution to address these challenges. The advent of Physics-Informed Neural Networks (PINN) has expanded the scope of Deep learning applications in turbulent flow modelling. However, applying PINN to complex flow physics within porous media remains an underexplored territory. This study employs PINN to solve the Reynolds-Averaged Navier-Stokes (RANS) equations in a composite porous-fluid system, guided by supervised learning and penalized by the RANS equation to ensure fidelity to flow physics. The research aims to enhance flow prediction accuracy and explore the influence of data distribution on PINN performance in complex flow scenarios in composite porous-fluid systems. Results showed that using porous-fluid interface training data provides better accuracy, with improvements of 40% and 2% in second-order statistics. This research contributes to advancing our understanding of turbulent flows in porous media and highlights the potential of PINN as a valuable tool for exploring complex flow physics.

Keywords**:** Porous flow; Physics-Informed Neural Networks (PINN); Turbulent flow; Reynolds-Averaged Navier-Stokes; Composite porous-fluid systems.

1. Introduction

The modelling of porous media is a big challenge in the field of Computational Fluid Dynamics (CFD) due to its inherent complex fluid dynamics. Since porous media have been largely implemented in heat and mass transfer systems such as interstitial fluids in microbiology, natural convection in building and geothermal sciences, the importance of physical analysis of the behaviour of fluids within structures has been highlighted [1-3]. This inherent structure provides unique flow behaviour within and around a porous block in a composite porous-fluid system [4-5]. Within this system, flows can be categorized into two primary regions: the non-porous region and the porous region, separated by a porous-fluid interface (see Fig. 1). In this system, the presence of high-velocity gradients and flow variations over the porous media determine the characteristics of the fluid behaviour [5]. In Fig. 1 upstream of the block in Region I, laminar flow prevails. Region II, on the other hand, is characterized by flow separation, manifesting as vortical structures leading to flow recirculation and boundary layer redevelopment. Notably, a free shear layer forms at the interface of the blockage within this region. In Region III, downstream of the block, flow separation reoccurs, resulting in reversed flow that subsequently reattaches and develops further downstream in the wake. Lastly, in Region IV, flow leakage phenomena [6] occur due to the porous structure of the bluff body.

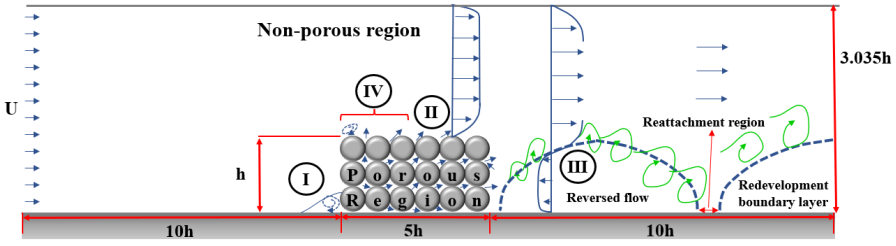

Fig. 1: Schematic diagram of fluid behaviour in the composite porous-fluid system which consists of a fluid-saturated porous block and a turbulent flow passing over it [5].

Due to those complex structures, capturing the flow between porous and non-porous regions proves to be a challenge. Although there have been pore-scale [5] and volume-averaged [7] modelling strategies that analyse turbulent properties such

as Reynolds stresses or turbulent viscosity, those approaches have their disadvantages and cannot achieve accurate yet low-cost modelling. Furthermore, both in experimental and computational contexts, this multifaceted interaction has not been well-documented in the literature, highlighting the need for further investigation in this area employing state-of-the-art techniques and methodologies to advance our understanding of these complex phenomena [8].

In recent years, the implementation of Deep learning (DL) has been introduced to various engineering applications, and various DL architectures, including Fully Connected Neural Networks (FCNN), Convolutional Neural Networks (CNN) and Generative Adversarial Networks (GAN) has accelerated its application on the turbulence modelling [10-12]. With this realm of DL, the capabilities of modelling nonlinear relationships through the DL have gained the attention to solve the Partial Differential Equations (PDEs) that govern the flow physics with two distinct approaches: data-driven and physics-informed. While data-driven methods rely heavily on extensive training datasets for accurate predictions, they necessitate significant computational resources and may struggle to secure elaborate datasets in the modelling of complex flow physics [13]. In contrast, physics-informed deep learning incorporates the governing equations of physics into its models, leveraging physical laws to enhance modelling robustness [14-15]. The advent of Physics-Informed Neural Networks (PINNs) has helped in a new era of numerical modelling across engineering applications, spanning from solid materials to fluid dynamics [16-17]. Within the domain of fluid dynamics, while the effectiveness of PINNs in solving Navier–Stokes equations for laminar flows has been demonstrated in several studies [18-19], the utilization of PINNs to address turbulent flows with complex flow physics has garnered relatively scant attention in the literature [20].

Eivazi, et al. [21], successfully employed PINNs to solve the Reynolds-averaged Navier–Stokes (RANS) equations within specific subdomains. They trained a PINN to satisfy the RANS equations without relying on a transport-equation-based model to predict turbulent boundary layers. This approach was applied to high Reynolds number flows in a subdomain on an airfoil and flows over periodic hills. Xu, et al. [22] adopted a similar strategy, training a PINN to predict turbulent viscosity without imposing any specific equations. They calibrated their model using CFD data and leveraged it to explore missing flow information within a finite region downstream of a backwards-facing step. Hennigh, et al. [23] applied the mixing-length turbulence model to predict turbulent thermal flows using PINNsTheir results showcased the ability of PINN-inspired techniques to amplify finer turbulent scales beyond the capabilities of traditional interpolation methods while maintaining consistency with governing principles. Despite these notable advances in turbulence modelling, the application of PINNs to investigate complex flow physics within porous media remains a relatively unexplored domain.

This study aims to leverage Physics-Informed Neural Networks (PINNs) to solve the Reynolds-Averaged Navier-Stokes (RANS) equations within a composite porous-fluid system at the pore-scale level. The PINN model is trained while being constrained by the RANS equations to ensure fidelity to the underlying flow physics. The input features consist of spatial coordinates, while the output variables represent key flow parameters including the first- and second-order statistics. Boundary data and a limited set of training samples within the domain are provided. The reference data for mean flow quantities and Reynolds stresses components are derived from the RANS $k-\varepsilon$ model. The primary objectives of this study are: 1) To assess the capability of PINNs in modelling turbulent flows within a composite porous fluid system, which entails complex flow physics; 2) To investigate the impact of incorporating internal domain training data on the predictive accuracy of the PINN model. To achieve this, we compare the predictive accuracy of the PINN for both first-order and second-order statistical measures against CFD predictions. The analysis spans complex flow scenarios, including flow over porous blocks within the composite porous fluid system.

2. Methodology

In this section, the PINN for fluid mechanics is explained with the governing equation of the turbulent flow. Next, PINN architecture is described with the each term that consist of Neural Network (NN) loss function. In addition, the numerical configuration for the CFD and PINN training is illustrated.

2.1. Governing Equations

The Navier-Stokes and continuity equations govern the behaviour of most fluid flows. Nevertheless, the simulation of instantaneous flow phenomena across a wide range of time and length scales remains a challenge within traditional turbulence models. To overcome this problem, the flow variables that are implemented into the Navier-stokes equations are conducted with the time-averaging process which is called Reynolds decomposition [24]. This low-cost modelling is named as Reynolds Averaged Navier-Stokes (RANS) equation [25]. Without modelling the term of turbulent viscosity

(ν), direct Reynolds stress components are implemented to the governing equation. When the fluid is incompressible with steady turbulent flow. The RANS equation is presented below.

$$\frac{\partial \overline{u_i}}{\partial x_i} = 0 \tag{1}$$

$$\frac{\partial \overline{u_i}\,\overline{u_j}}{\partial x_j} + \frac{\partial \bar{p}}{\partial x_i} - \frac{\partial}{\partial x_j}\left(\nu \frac{\partial \overline{u_i}}{\partial x_j}\right) + \frac{\partial \overline{u'_i u'_j}}{\partial x_j} = 0 \tag{2}$$

where, $\bar{u}$ and $\bar{p}$ are time-averaged components, ν is kinematic viscosity, and $\overline{u'_i u'_j}$ is Reynolds stress components which are derived from Reynolds decomposition.

2.2. Physics Informed Neural Network (PINN)

Compared with the data-driven method for predicting the flow variables in various DL research, PINN combines the existence of a governing equation in the loss function with observation data [14,15,26]. This method is mesh-free which is fundamentally different from the conventional method, which requires the discretization of the governing equation along the meshes [24]. Moreover, the implementation of the governing equation makes predictions more reliable compared with a data-driven model. The PINN architecture in this study is shown below.

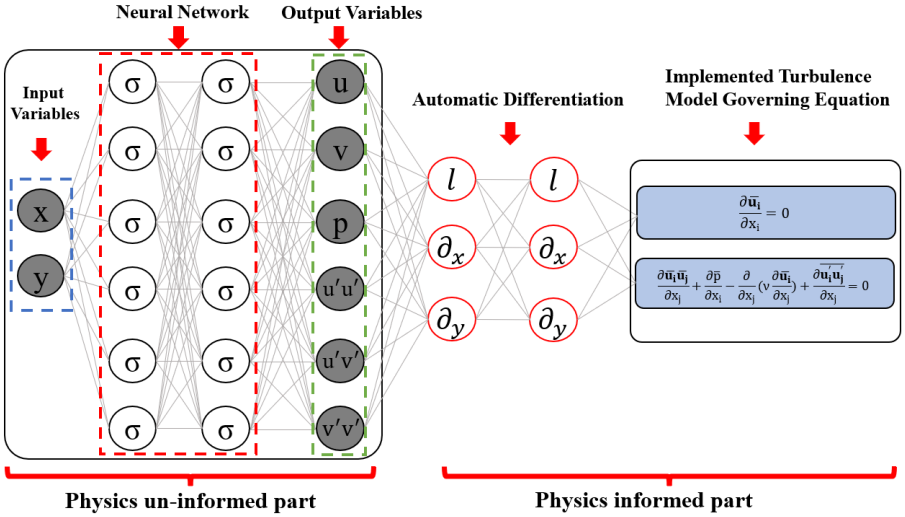

Fig. 2: PINN architecture with implemented governing equations.

The inputs of the PINN are spatial cartesian 2D coordinates, which are the input features of the given PDE. The Neural Networks (NN) structure is constructed with several hidden layers and neurons. The output variables are flow variables. Also, the governing equations relate to the derivatives of each output variable to make the architecture of PINN. The derivatives are calculated by Automatic Differentiation, which is an algorithmic technique that is used for calculating the value of its derivative inside of the hidden layers. The output vector of PINN in fluid mechanics is $\mathbf{u}(x, y)$, and non-linear operators are involved in the PDE, which is presented in Equation (3). Based on this equation, the loss function of PINN is minimized in the direction of optimizing the parameters that construct the NN architecture.

$$\mathbf{u}(x, y) + \mathcal{N}[\mathbf{u}] = 0 \tag{3}$$

$$\mathcal{L} = |\hat{\mathbf{u}} - \mathbf{u}| + |\mathcal{N}[\hat{\mathbf{u}}]| \tag{4}$$

where, $\hat{\mathbf{u}}$ is the predicted value of the PINN and $\mathbf{u}$ is the training dataset for supervised learning. The loss function of the PINN is constructed with several terms. Based on the spatial coordinates $x, y \in R$ where R is the training domain. The

governing equations is constructed by PDE loss, the Dirichlet and Neumann boundary conditions for the PDE make boundary condition loss, the Initial condition which has a solution of PDE at the beginning of time is an initial condition loss. Lastly, the discrepancy of value between the observational data and the inferred solution is a data loss. Those losses make a total loss, which must be minimized during the training. To measure the criteria for this loss, the Mean Squared Error function is generally used in the PINN. The loss terms that compose the PINN are described below. The equation (1) and (2) are implemented as the PDE loss term [15]. However, in the developed methodology in the present study PINN training, $\mathcal{L}_{IC}$ and $\mathcal{L}_{BC}$ are not implemented into the loss function during the training. Because, first, the flow scenario is assumed to be a steady state. Second, different from the conventional CFD simulation, PINN boundary condition of the turbulent properties such as Reynolds stresses ($\overline{u'u'}$, $\overline{v'v'}$, $\overline{u'v'}$) are difficult to define in fixed value or pre-defined assumptions. Therefore, for those boundary condition loss ($\mathcal{L}_{BC}$) is substituted into $\mathcal{L}_{Data}$ that relies on the provided labelled data in the PINN training.

$$\mathcal{L} = w_1 \times \mathcal{L}_{PDE} + w_2 \times \mathcal{L}_{Data} \tag{5}$$

where the $w_{1\text{-}2}$ are the weighting coefficients which balance the importance of each loss factor to minimize the total loss.

$$\mathcal{L}_{PDE} = \frac{1}{N}\sum_{i=1}^{3}\sum_{n=1}^{N} |e_i^n|^2 \tag{6}$$

$$\mathcal{L}_{Data} = \frac{1}{N_{Data}}\sum_{i=1}^{N_{Data}} |\mathbf{u}_{Data}{}^i - \hat{\mathbf{u}}_{Data}{}^i|^2 \tag{7}$$

2.3. Numerical Configuration

The training dataset is generated by the OpenFOAM v2012 for numerical calculation. The geometry is shown in Fig.3. The case has 36.38 % porosity (φ) with a 30 mm diameter of porous structures. The Reynolds number (Re) of flow is targeted to 5600, ensuring the vortex structure on top and inside of the porous structure. To analyse turbulent flow, the $k-\varepsilon$ modelling [25] is used to confirm the low cost, yet acceptable range of prediction of the porous structure. "SimpleFoam" is implemented to solve the steady-state turbulent flow [27]. After solving the numerical scheme, the Reynolds stress components are calculated with a built-in postprocessing function in the OpenFOAM v2012 [27].

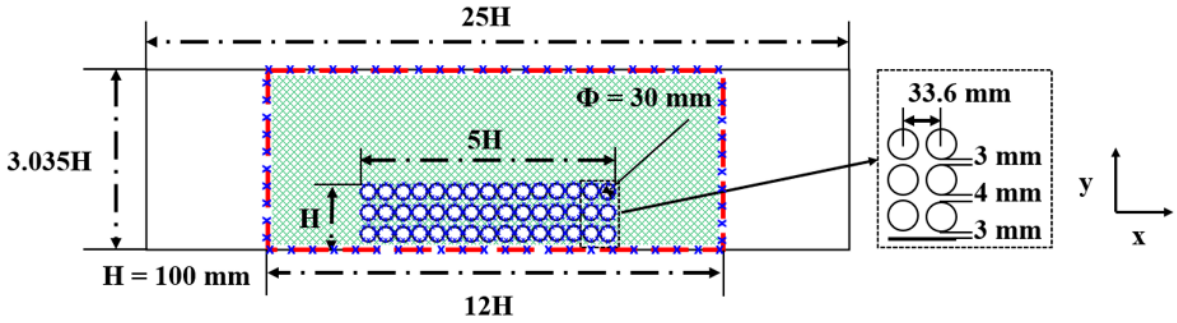

Fig. 3: Geometry of porous block with cubic packed arrangement formed from circular cylinders; (Porosity(φ) = 36.38%, D = 30 mm).

Based on the post-processed data, the region where the flow over the bluff body has distinct flow features such as recirculation and reverse flow is extracted to train the PINN. For the base PINN training, only the boundary data is given during the training. The PINN training incorporates an adaptive weight strategy based on the neural tangent kernel (NTK) to mitigate any potential spectral biases introduced during training [28].

3. Discussion of Results

The results obtained by PINN prediction for the porous cases in the composite porous-fluid system are presented in this section. Three different scenarios for PINN training are considered in the present paper: (i) Case G0 represents the base scenario, which utilizes only boundary data for training. In the case of G0 shown in Fig. 4 (a), four different zones show flow physics similar to those discussed in Figure 1, with Zone IV standing out due to its distinct features, including flow leakage [6] and a channelling effect [5] around the porous media. (ii) Case G1 involves guideline data at the porous-fluid interface. (iii) Case G2 is similar to G1 but does not include training data at the porous-fluid interface. Comprehensive analyses, including quantitative and qualitative discussion, are evaluated through a range of diverse flow visualization techniques and

calculations. This examination encompasses a thorough assessment of first and second-order statistics, providing insights to offer a broad understanding of the predictive performance of the PINN model. The error is quantified using the L_2 relative norm error ($||\Phi_{CFD}-\Phi_{PINN}||_2/||\Phi_{CFD}||_2$, where $||\ldots||_2$ is Euclidian norm and Φ is flow variables) and the local region L_2 errors. It is essential to note that all reference data utilized in this analysis is sourced from RANS CFD data, ensuring the reliability and consistency of the benchmark data for evaluation. To accommodate the complexity of the geometry, both first-order and second-order flow statistics are incorporated into the training process to ensure reasonable accuracy.

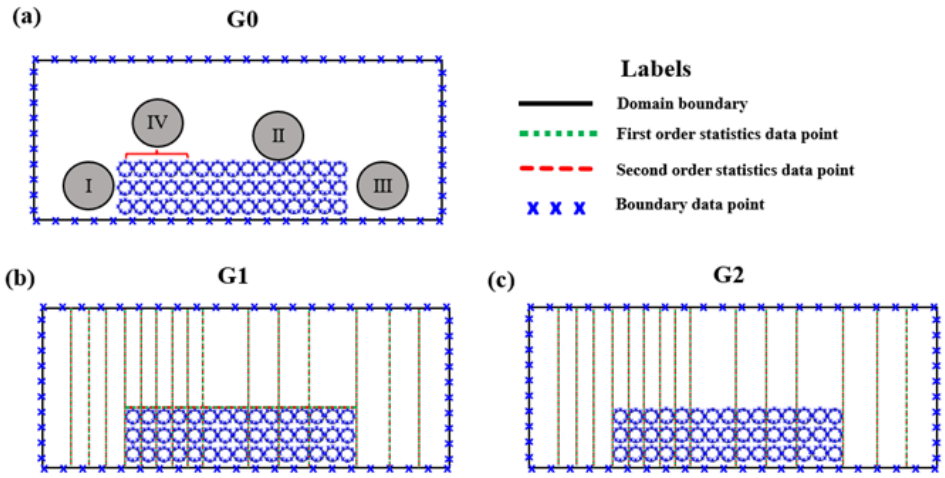

Fig. 4: Three different scenarios for PINN training; (a) Case G0 represents the base scenario, which utilizes only boundary data for training. (b) Case G1 involves training data at the porous-fluid interface. (c) Case G2 is similar to G1 but without training data at the porous-fluid interface.

Fig. 5 shows the comparison of first and second-order statistics based on different scenarios (see Fig.4) for PINN training. As depicted in Fig. 5, the results of the G0 case exhibited distinct features for all flow variables when compared to the reference data. When considering mean flow variables (first-order statistics), the results for the case without training data (G0) exhibited discrepancies compared to the reference data. These discrepancies were particularly noticeable in Region I, where there was overprediction in both streamwise and vertical directions. Additionally, in the pressure field, there was a discontinuity in the precision of pressure in the stagnation region, which appeared to be inaccurate when compared to the reference data. Regarding second-order statistics, PINN, without any training data in the internal domain, struggled to accurately predict the disturbance in Reynolds stress ($\overline{u'v'}$). Results from the case that incorporate internal and porous-fluid interface data (G1) for training PINN demonstrated improved agreement with the reference pressure and streamwise velocity outcomes. However, accurate prediction of $\overline{u'v'}$ remained a challenge. Finally, in the case that utilizes only training data along the vertical line (G2), rather than at the porous-fluid interface, the trends for $\overline{u'v'}$ closely resembled the reference predictions. However, there was a notable discrepancy in the accuracy of predicting the magnitude of $\overline{u'v'}$.

Table I presents a comparative analysis of results for three distinct scenarios used in the training of PINNs, as illustrated in Figure 4. Notably, the L_2 error for all flow variables in scenario G0 was noticeably less accurate when contrasted with the other two scenarios. However, when the data was introduced into the training process for scenarios G1 and G2, the PINN demonstrated an enhanced ability to capture the intricate flow dynamics within the flow domain. In particular, when compared to scenario G0, this augmentation of data significantly improved the accuracy of Reynolds stresses. This underscores the critical importance of incorporating internal flow information for the porous structure that induces complex flow behaviour, as it leads to markedly superior accuracy in modelling.

When comparing the G1 and G2 cases in L_2 error for the total flow domain, contrary to the conclusion drawn from Fig. 5, G1, which includes interface conditions, yielded better results in terms of prediction accuracy for the turbulent properties. However, when examining the regional L_2 norm error for these two cases, the superiority of this case was not distinguished with minimal differences in the result, meaning the presence of interface training data did not significantly impact Zone I to III. Nonetheless, in Zone IV, where the fluid flow changed most noticeably, G1 exhibited better accuracy in second-order statistics than G2. This suggests that implementing interface conditions in complex flow region affects the accuracy of flow

characteristics within the porous structure, and this provided a good agreement for predicting flow leakage phenomena. In conclusion, when there was no significant alteration in flow behaviour, the inclusion of interface data did not greatly impact prediction accuracy, as evidenced by the regional L_2 norm error in Table I. However, for the dynamic flow behaviour region, utilizing interface training data in the G1 case resulted in a superior accuracy compared to the non-interface G2 case, with differences of 40% and 2% observed for second-order statistics.

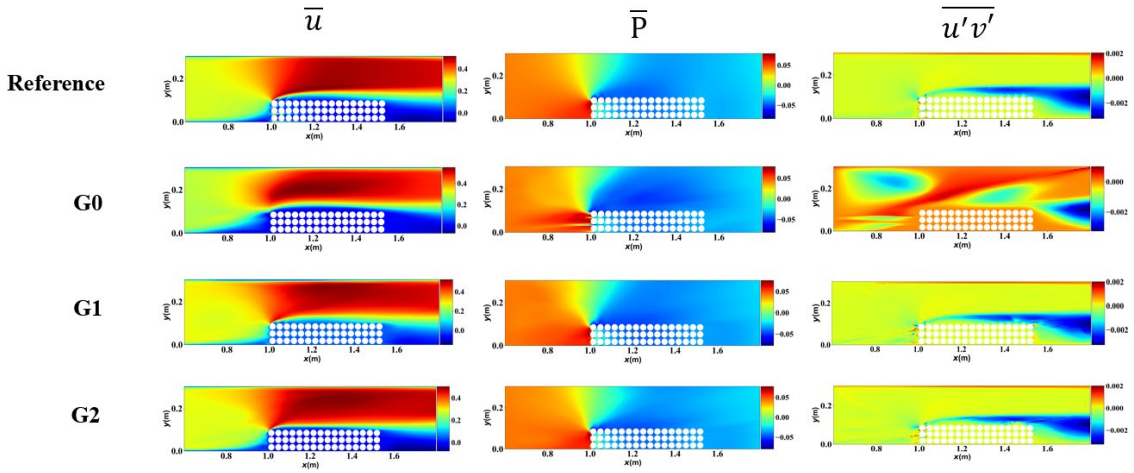

Fig. 5: The comparison of first and second-order statistics based on different scenarios for PINN training, as previously explained in Fig. 4; row 1: Reference results; row 2: G0 scenario; row 3: G1 scenario; row 4: G2 scenario.

Table 1: L_2 norm error for the entire PINN domain for first and second-order statistics and regional L_2 norm error for specified flow physics zone with different training data guidelines scenarios as previously explained in Fig. 4.

Variables	**Total Region Relative L_2**		
	G0	**G1**	**G2**
$\overline{u}$	16.18 %	7.02 %	6.42 %
$\overline{\mathrm{P}}$	16.94%	1.66%	1.43 %
$\overline{u'u'}$	388.67%	18.04 %	25.30%
$\overline{u'v'}$	86.90%	19.94 %	20.80%

Variables	**Regional Relative L_2**							
	I		**II**		**III**		**IV**	
	G1	**G2**	**G1**	**G2**	**G1**	**G2**	**G1**	**G2**
$\overline{u}$	3.71%	4.26%	0.78 %	1.17%	15.32%	16.73%	67.96%	59.49%
$\overline{\mathrm{P}}$	2.51%	1.07%	0.68%	1.04%	0.92%	2.41%	3.62 %	2.69%
$\overline{u'u'}$	72.14%	120.12%	3.17%	3.05%	4.79%	5.85%	19.22%	55.08%
$\overline{u'v'}$	109.09%	72.04%	10.52%	16.64%	12.56%	8.60%	76.34%	78.24%

where, $\overline{u}$ is mean streamwise velocity, $\overline{\mathrm{P}}$ is pressure, $\overline{u'u'}$ and $\overline{u'v'}$ are Reynolds normal and shear stresses, G0 is base scenario with only boundary data, G1 is second scenario with porous-fliud interface and G2 is third scenario without training data at the porous-fluid interface.

Vertical distributions of streamwise velocity ($\overline{u}$) through and above the porous region were compared with the reference case in Fig. 6. Strong negative streamwise velocity at X/H = 1.0 confirmed the presence of primary recirculation region on the porous-fluid interface. Below the interface in the porous region, the velocity profiles had a non-uniform wavy shape due to the geometric characteristics of the pores and they continuously experienced acceleration and deceleration due to contractions and expansions of the flow as they pass through the pores. Moreover, Fig. 6 (b) and (c) shows a drop in the maximums of streamwise velocity below the interface. Although there was a less distinguished feature in both graphs in Fig.

6 (b) and (c), the black dashed circle inside of the porous region showed that the interface condition gives better accuracy of the streamwise velocity profile.

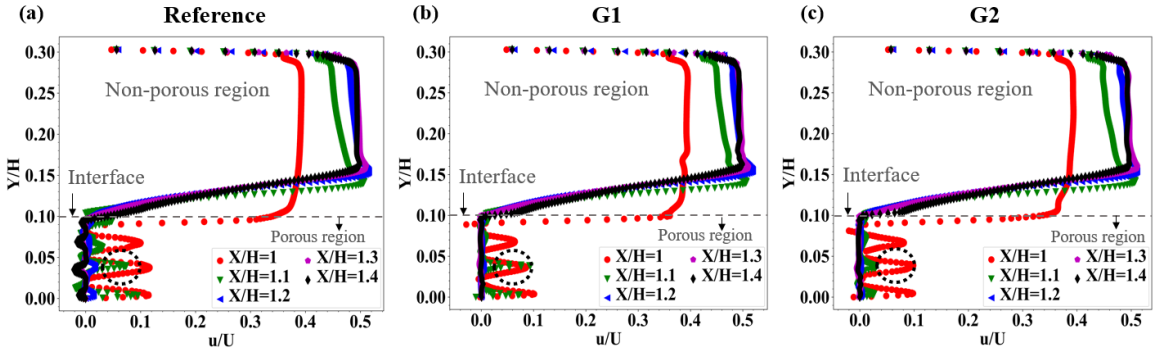

Fig. 6: Vertical distribution of streamwise velocity on the streamwise direction of the porous structure (a) reference data; (b) interface training data included case (G1); (c) without interface training data case (G2).

4. Conclusion and future work

The utilization of Physics-Informed Neural Networks (PINN) for predicting turbulent flows in porous media represents a challenging yet promising approach for numerical simulations of fluid and heat transfer. Although PINN has demonstrated the capability to achieve accurate predictions for laminar flows without the need for labelled training datasets, accurately predicting turbulent flows, particularly for second-order statistics, in the absence of labelled data remains an ongoing challenge. This research has illuminated the difficulties associated with predicting turbulent flows and second-order statistics, especially in scenarios featuring composite porous-fluid systems, where accurate prediction of turbulence statistics remains a challenge. To address these challenges, we introduced a data augmentation method, which yielded improved predictions when compared to other configurations without training data in the internal domain. The result showed the training with data from the porous-fluid interface increaseed the prediction accuracy. Moreover, the regional L_2 norm error showed that where there is no noticeable change of flow heavier, prediction accuracy was not highly affected by the interface data augmentation. However, in the region with high values of flow leakage, interface training data in G1 provided better accuracy compared with G2 by 40 % and 2 % difference for second-order statistics. The research will provide in-depth understanding of turbulent flows in porous media by corporating the potential of PINN to more complex flow physics.

Acknowledgements

Data supporting this publication can be obtained on request. The authors would like to acknowledge the assistance given by Research IT and the use of the Computational Shared Facility at The University of Manchester.

References

[1] M. S. Kandelousi and D. D. Ganji, "Flow and heat transfer in porous media," in *Hydrothermal Analysis in Engineering Using Control Volume Finite Element Method*, Babol, Academic Press, 2015, pp. 177-210.

[2] A. A. Mohamad, "Combustion in Porous Media: Fundamentals and Applications," in *Transport Phenomena in Porous Media III*, Calgary, Pergamon, 2005, pp. 287-304.

[3] D. Pokrajac, C. Manes and I. McEwan, "Peculiar mean velocity profiles withnin a porous bed of an open channel," *Physics of Fluids*, 2007, vol. 098109, pp. 19.

[4] M. Jadidi, H. K. Param, and Y. Mahmoudi, "On the mechanism of turbulent heat transfer in composite porous-fluid systems with finite length porous blocks: Effect of porosity and Reynolds number," *International Journal of Heat and Mass Transfer*, 2023, vol. 208, pp. 124006.

[5] M. Jadidi, A. Revell, and Y. Mahmoudi, "Pore-scale large eddy simulation of turbulent flow and heat transfer over porous media," *Applied Thermal Engineering*, 2022, vol. 215, pp. 118916.

[6] M. Jadidi, H. K. Param, A. Revell, and Y. Mahmoudi, "Flow leakage and Kelvin–Helmholtz instability of turbulent flow over porous media," *Physics of Fluids*, 2022, vol. 34, no. 10.

[7] Y. Mahmoudi and N. Karimi, "Numerical investigation of heat transfer enhancement in a pipe partially filled with a porous material under local thermal non-equilibrium condition," *International Journal of Heat and Mass Transfer*, vol. 68, pp. 161-173.
[8] P. Kundu, V. Kumar, Y. Hoarau and I. M. Mishra, "Numerical simulation and analysis of fluid flow hydrodynamics through a structured array of circular cylinders forming porous medium," *Applied Mathematical Modelling*, 2016, vol. 40, pp. 9848-9871,.
[9] C. Jiang, C. Jiang, D. Chen and F. Hu, "Densely Connected Neural Networks for Nonlinear Regression," *Entropy*, 2022, vol. 24, no. 7, pp. 876.
[10] S. Srivastava and K. C. Tripathi, "Artificial Neural Network and Non-Linear Regression: A Comparative Study," *International Journal of Scientific and Research Publications*, 2012, vol. 2, no. 12, pp. 740-744.
[11] A. Aggarwal, M. Mittal and G. Battineni, "Generative adversarial network: An overview of theory and applications," *International Journal of Information Management*, 2021, vol. 1, no. 1, pp. 100004.
[12] J. Gui, Z. Sun, Y. Wen, D. Tao and J. Ye, "A Review on Generative Adversarial Networks: Algorithms, Theory, and Applications,",2020, *arXiv*:2001.06937.
[13] S. Guo, M. Agarwal, C. Cooper, Q. Tian, R. X. Gao and W. G. Grace, "Machine learning for metal additive manufacturing: Towards a physics-informed data-driven paradigm," *Journal of Manufacturing System*, 2022, vol. 62, pp. 145-163.
[14] M. Raissi, P. Perdikaris, and G. E. Karniadakis, "Physics-informed neural networks: A deep learning framework for solving forward and inverse problems involving nonlinear partial differential equations," *Journal of Computational Physics*, vol. 378, pp. 686-707.
[15] X. Jin, S. Cai, H. Li, and G. E. Karniadakis, "NSFnets (Navier-Stokes flow nets): Physics-informed neural networks for the incompressible Navier-Stokes equations," *Journal of Computational Physics*, vol. 426, pp. 109951.
[16] D. Amini, E. Haghighat and R. Juanes, "Physics-Informed Neural Network Solution of Thermo–Hydro–Mechanical Processes in Porous Media," *Journal of Engineering Mechanics*, 2022, vol. 148, no. 11.
[17] E. Haghighat, A. C. Bekar, E. Madenci and R. Juanes, "Deep learning for solution and inversion of structural mechanics and vibrations," in *Modeling and Computation in Vibration Problems*, vol. 2, IOP publishing, 2021, pp. 1-17.
[18] V. Sekar, Q. Jiang, C. Shu and B. C. Khoo, "Accurate near wall steady flow field prediction using Physics Informed Neural Network (PINN),", 2022, *arXiv*:2204.03352.
[19] H. Bararnia and M. Esmaeilpour, “On the application of physics informed neural networks (PINN) to solve boundary layer thermal-fluid problems,” *International Communications in Heat and Mass Transfer* , 2022, vol. 132, no. 8, pp. 105890.
[20] P. Y. Chuang and L. A. Barba, "Predictive Limitations of Physics-Informed Neural Networks in Vortex Shedding," , 2023, *arXiv*:2306.00230.
[21] H. Eivazi, M. Tahani, P. Schlatter, and R. Vinuesa, "Physics-informed neural networks for solving Reynolds-averaged Navier–Stokes equations," *Physics of Fluids*, vol. 34, no. 7.
[22] H. Xu, W. Zhang, and Y. Wang, "Explore missing flow dynamics by physics-informed deep learning: The parameterized governing systems," *Physics of Fluids*, vol. 33, no. 9
[23] O. Hennigh, S. Narasimhan, M. A. Nabian, A. Subramaniam, K. Tangsali, Z. Fang, M. Rietmann, W. Byeon and S. Choudhry, "NVIDIA SimNet™: An AI-Accelerated Multi-Physics Simulation Framework," Cham, 2021: *Springer International Publishing, in Computational Science* – ICCS 2021, pp. 447-461.
[24] H. K. V. Malalasekera and W, *An introduction to computational fluid dynamics: the finite volume method*. Pearson Prentice Hall, 2007.
[25] S. B. Pope, *Turbulent Flows*. Cambridge: Cambridge University Press, 2000.
[26] E. Haghighat and R. Juanes, "SciANN: A Keras/TensorFlow wrapper for scientific computations and physics-informed deep learning using artificial neural networks," *Computer Methods in Applied Mechanics and Engineering*, vol. 373, pp. 113552.
[27] H. G. Weller, G. Tabor, H. Jasak, and C. Fureby, "A tensorial approach to computational continuum mechanics using object-oriented tetechniques," *Computer in Physics*, vol. 12, no. 6, pp. 620-631.
[28] S. Wang, X. Yu and P. Perdikaris, "When and why PINNs fail to train: A neural tangent kernel perspective," *Journal of Computational Physics*, 2022, vol. 449, pp. 110768.